Estimation of Monthly Rainfall over Oceans from Truncated Rain-Rate Samples: Application to SSM/I Data

YE HONG,* THOMAS T. WILHEIT, AND WILLIAM R. RUSSELL

Department of Meteorology, Texas A&M University, College Station, Texas

(Manuscript received 19 October 1996, in final form 22 November 1996)

ABSTRACT

A physical–statistical monthly rainfall retrieval algorithm has been developed using multichannel brightness temperatures from the Special Sensor Microwave/Imager (SSM/I). Since an emission-based retrieval algorithm gives the most physically direct estimation of rainfall over oceans, instantaneous rain rates are retrieved using brightness temperature–rain rate (T–R) relationships derived from a radiative transfer model. The retrieved rain rates, however, are only reliable and useful over a portion of a whole dynamic range of rain rate due to limitations of the emission-based algorithm. When monthly rainfall in a $5^\circ \times 5^\circ$ box is estimated, the instantaneous rain-rate samples are actually truncated. The method used in this study assumes that monthly rainfall intensity in a $5^\circ \times 5^\circ$ box has a mixed lognormal distribution. Thus, the contribution of the rain rates outside of the dynamic range can be estimated by extrapolation. Coefficients of the mixed lognormal distribution are determined by fitting the truncated rain-rate samples to the lognormal form using a maximum likelihood estimate method. The beamfilling error is corrected by a multiplicative factor generated from simulation studies. Comparison between the monthly rainfall estimated from the SSM/I and Pacific atoll data indicates that the algorithm works very well in tropical areas. Although this algorithm is tested on SSM/I data, it is also suited for the Tropical Rainfall Measuring Mission data, which should have a larger dynamic range with 10.7-GHz channels added.

1. Introduction

Rainfall is the primary exchange process within the hydrological cycle. The latent heat released by tropical rainfall plays a crucial role in driving the low-latitude atmospheric circulation. Because of the huge extent of oceans, very little oceanic rainfall data are available from measurements by rain gauges, surface-based radar, and other conventional means. Satellite observation is considered the most reasonable method for oceanic rainfall measurement. Therefore, accurate estimates of rainfall based on satellite-derived data are necessary. They will improve the inputs to climate models and global circulation models and hence will improve our understanding of large-scale climate variability and our knowledge of the workings of the earth–atmosphere–hydrosphere system.

A series of satellites that carried visible–IR imagers or microwave radiometers have been used for detecting global rainfall. One of those is the Special Sensor Microwave/Imager (SSM/I) on the Defense Meteorological Satellite Program (DMSP) polar orbiting satellite, which was first launched in June 1987. It is a seven-channel, four-frequency (19.35, 22.235, 37.0, and 85.5 GHz) microwave radiometer that measures atmospheric–ocean surface brightness temperatures in both horizontal and vertical polarizations at all frequencies except 22.235 GHz, for which there is only a vertically polarized channel. The very clean design of the SSM/I has resulted in very stable, well-calibrated measurements. The operational nature of the DMSP satellite series has resulted in a reliable quasi-continuous data source. Although its spatial resolution at the lowest-frequency channel is rather poor, the SSM/I has been the most useful microwave instrument to date for rainfall estimation.

The proposed Tropical Rainfall Measuring Mission (TRMM) satellite (Simpson et al. 1988) is scheduled to be launched in 1997. The TRMM payload will include the TRMM Microwave Imager (TMI), which is essentially a copy of the SSM/I with a dual-polarized pair of 10.7-GHz channels added. One of the principal goals of TRMM is to determine the distribution and variability of rainfall and latent heat release on a monthly, $5^\circ \times 5^\circ$ basis over the tropical oceans. It was this goal of TRMM that prompted us to develop the monthly rainfall estimation algorithm based on the SSM/I data.

Passive microwave rainfall-rate retrievals are usually based on one of two approaches (Wilheit 1986), although a few algorithms use both. The first method is emission-based, where absorption and emission by liq-

* Current affiliation: Caelum Research Corporation, Silver Spring, Maryland.

Corresponding author address: Dr. Ye Hong, NASA/GSFC, Code 912, Greenbelt, MD 20771.
E-mail: yhong@audry.gsfc.nasa.gov

uid cloud drops and raindrops cause rapid increases of brightness temperatures over a radiometrically cold background, such as the ocean. Most emission-based approaches rely on integration of the equation of radiative transfer for hypothetical models of raining atmosphere to predict the brightness temperature for a given rainfall rate. This method was first explored by Wilheit et al. (1977) and has been used by Weinman and Guetter (1977), Huang and Liou (1983), Wu and Weinman (1984), Olson (1987), Kummerow and Weinman (1988), Smith and Mugnai (1988), Mugnai and Smith (1988), and many others.

The second approach is scattering based, where scattering by ice hydrometeors in the upper parts of clouds causes brightness temperature decreases over land or ocean. Using airborne radiometers, Wilheit et al. (1982) first observed brightness temperatures as low as 140 K at 92 GHz and near 183 GHz over convective elements of Tropical Storm Cora. Scattering-based approaches are generally empirically based statistical relationships between satellite-measured brightness temperatures and surface rain rates, which are obtained from coincident ground-based radar measurements. Spencer et al. (1983) first used this approach to retrieve rain rates from the *Nimbus-7* Scanning Multichannel Microwave Radiometer (SMMR) 37-GHz data. Rodgers and Siddalingaiah (1983), Spencer (1986), Spencer et al. (1989), and Petty and Katsaros (1990) have used different statistical relationships to retrieve rainfall over ocean and land.

Recently, Kummerow et al. (1989) and Kummerow et al. (1991) have developed a multichannel statistical–physical rain-rate retrieval approach. They established the statistical relationships between multichannel brightness temperatures and rain rates based upon data generated by a cloud radiative model for a wide range of conditions. The model simulates various atmospheric parameters, cloud structures, cloud microphysics, and surface characteristics and then computes their associated brightness temperatures in each of the available channels. Those simulated parameters are adjusted to obtain consistency between observed and calculated brightness temperatures. More recently, Kummerow and Giglio (1994a,b) improved this approach by explicitly accounting for diverse hydrometeor profiles. As a result, potential errors introduced into the theoretical calculations by the unknown vertical distribution of hydrometeors are reduced. Using similar techniques, Olson (1989), Smith et al. (1992), and Mugnai et al. (1993) have retrieved rain rates by employing different cloud models.

Algorithms for estimating area–time-averaged rainfall from satellite measurements have been developed for climatological studies. Shin et al. (1990) retrieved seasonal $5^\circ \times 5^\circ$ area-averaged rain rate over the tropical oceans by using single-channel microwave measurements from ESMR-5. Wilheit et al. (1991) developed an algorithm for the estimation of monthly rain totals for $5^\circ \times 5^\circ$ cells over the oceans from SSM/I brightness temperatures. A linear combination of the 19.35- and 22.235-GHz channels was adopted to reduce the impact of the variability of water vapor. A mixed lognormal distribution was assumed as the probability distribution function of rainfall intensity. The coefficients of the mixed lognormal distribution were determined by matching the observed histogram of brightness temperature with the predicted histogram. Berg et al. (1992) computed monthly, seasonal, and annual oceanic rainfall from the SSM/I using a mixed lognormal distribution. They used the Hughes D-matrix algorithm to estimate the instantaneous rainfall and summed it over $1^\circ \times 1^\circ$ box for each month. Then the ensemble of instantaneous rainfall values was fitted to a lognormal distribution by using a maximum likelihood method.

The previous work for estimating area–time-averaged rainfall has assumed that rain rates over whole dynamic range are available. However, this assumption is not true because an emission-based rain-rate retrieval has its limitations. First, the nonprecipitating clouds and water vapor will introduce the uncertainties in the estimates of low rain rates. Second, high rain rates cannot be retrieved due to the saturation of brightness temperatures. Even with a perfect measurement technique, the very high rain rates will also be poorly sampled with observations from a low orbiting satellite because of their relative infrequency. Thus, rain rate is reliably estimated only over a limited dynamic range so that only a portion of rain rates can be used in the estimation of monthly rainfall. In other words, when area–time-averaged rainfall is estimated, the instantaneous rain-rate samples are truncated. This study tries to get the best estimation of area–time-averaged rainfall from the truncated rain-rate samples.

The approach presented in this study still uses the emission-based method to retrieve instantaneous rain rates because the scattering-based algorithms work on a very tenuous physical connection. McGaughey et al. (1996) found that ice scattering in regions of convective precipitation over oceans during the Tropical Ocean Global Atmosphere Coupled Ocean–Atmosphere Response Experiment (TOGA COARE) was not as strong as those measured in convection over land. They also found that in tilted convective systems, there was ice aloft in stratiform regions with only light rain below and shallow heavily raining clouds with little ice above. Although scattering-based algorithms would extend the dynamic range of the measurements to higher rain rates, we do not have any confidence that the scattering can be related uniquely to rain rate.

The emission-based method gives the most physically direct estimate of rainfall over oceans because it represents observations of the liquid hydrometers. Its limitations can be overcome in the estimate of monthly rainfall by applying the maximum likelihood estimation algorithm to the truncated rain-rate samples; a brief description of data is given in section 2. The algorithm is described in detail in section 3. Section 4 applies this

algorithm to the SSM/I data and provides the comparison between satellite estimated monthly rainfall with the Pacific atoll data. A summary and conclusions are given in section 5.

The algorithm discussed in this paper is a refinement of the Wilheit et al. (1991). It differs in the following ways.

1) The brightness temperatures are converted into rain rates (and freezing levels) on a pixel-by-pixel basis before accumulation into histograms.
2) The parameters of the lognormal distribution of rain rates are found by a maximum likelihood estimator that takes the limited dynamic range of the measurements into account as opposed to the ad hoc method of estimation used by Wilheit et al. (1991).
3) The 37-GHz observations are used, albeit in an approximate manner, to extend the dynamic range to somewhat lower rain rates.

Note that the algorithm is the same as Wilheit et al. (1991) in two important respects. The underlying radiative transfer model and the beamfilling correction are unchanged. Recent research (Tesmer 1995; Wang 1996) has suggested improvements in both these areas. Tests of these presumed improvements are under way and will be reported at a later date.

2. Data

The satellite data used in this study are brightness temperatures from SSM/I for the months of August through December 1987 and January through December 1989. The SSM/I data have been described in detail by Hollinger et al. (1987). Only data from 50°N to 50°S were extracted. The brightness temperatures with bad geolocation data have been removed. Bad brightness temperature data, such as data from a single scan line over ocean with unexpected high values, were also eliminated from the data file.

The brightness temperatures from three channels (19-, 22-, and 37-GHz vertical channels) are applied in the retrieval of rain rate. For convenience, the brightness temperatures for those channels will be referred to T_{B19V}, T_{B22V}, and T_{B37V}, and rain rates retrieved from the corresponding channels will be R_{19V}, R_{22V}, and R_{37V}, respectively.

The validation data used here are the Pacific atoll rain gauge data provided by Morrissey et al. (1991). The atoll rain gauge data are little affected by topography and can represent open-ocean conditions. The monthly rain gauge totals were collected from 88 stations in the tropical Pacific and covered periods from January 1971 through December 1990. Only months with complete data were included. Months with missing data were excluded and accounted for about 30% of the total data. Unfortunately, the missing data made validation of monthly rainfall for 1989 difficult.

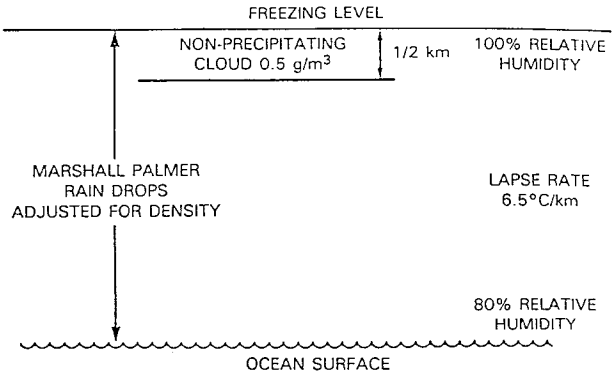

FIG. 1. Schematic diagram of the Wilheit et al. (1977) radiative transfer model.

3. Algorithm

a. Retrieval of instantaneous rain rate

Instantaneous rain rates are estimated from brightness temperatures using *T–R* relationships derived from the Wilheit et al. (1977) radiative transfer model. Figure 1 shows the schematic diagram of the radiative transfer model. In this model, a Marshall–Palmer (M–P) drop size distribution is assumed from the surface to the freezing level. The lapse rate is assumed to be 6.5 K km^{-1}, and the relative humidity is assumed to be 80% at the surface, to increase linearly to 100% at the freezing level, and remain at 100% above the freezing level. Thus, the freezing level serves as a proxy variable for both the rain-layer thickness and for the atmospheric water vapor content. In addition to the M–P distribution of rain drops, a nonprecipitating cloud layer containing 0.5 g m^{-3} of cloud liquid water is assumed in the 0.5 km just below the freezing level.

An analytical approximation to the *T–R* relationships for different SSM/I channels has been developed by Wilheit et al. (1991) and can be expressed as follows:

$$T(r) = T_0 + (285 - T_0)\left[1 - \exp\left(-\frac{r}{r_f}\right)\right] - ar^{1/2}, \quad (1)$$

where

$$r_r = \frac{b}{F^c}, \quad (2)$$

where $T(r)$ is measured brightness temperature, r is rain rate, F is the freezing level, and T_0 is the background temperature, which can be expressed as

$$T_0 = \mathrm{ta} + \mathrm{tb}F + \mathrm{tc}F^2.$$

The parameters a, b, c, ta, tb, and tc vary with different channels and are given in Table 1. These numbers are fits to computational results from the Wilheit et al. (1977) model. Here, F can be derived from T_{B19V}, T_{B22V}, and the *T–R* relationships using an iterative technique (Wilheit et al. 1991).

Applying the *T–R* relationships, instantaneous rain

TABLE 1. Constants for *T–R* relationships.

	19V	19H	22V	37V	37H
ta	172.0	104.5	167.2	212.7	156.6
tb	3.2	5.0	15.6	−1.1	−1.0
tc	1.65	2.33	0.68	1.12	1.60
a	3.5	3.5	3.7	6.0	6.0
b	21.2	19.2	19.0	6.5	5.8
c	1.20	1.03	1.40	1.15	1.00

rates can be retrieved from brightness temperatures for different channels. Figure 2 shows a freezing level–rain rate–brightness temperature (FLRRT) chart portraying a 2D histogram of brightness temperatures from the 19V and 22V channels over a 5° × 5° box in the intertropical convergence zone (ITCZ). Most pixels do not contain any rain, and the raining pixels are mainly located near the 4- and 5-km freezing levels.

Figure 3 shows the two *T–R* relationship curves for the 19V and 37V channels with a 4-km freezing level. As the rain rate increases, T_{B37V} increases faster at lower rain rates than does T_{B19V}. The T_{B37V} also saturates quickly at about 4.0 mm h^{-1}, whereas T_{B19V} reaches the maximum at about 12.0 mm h^{-1}. Thus, the 37-GHz channel is more sensitive to low rain rates, while 19 GHz has a larger dynamic range at the high-rain-rate end. To take advantage of both T_{B19V} and T_{B37V}, a composite best estimate of the rain rates is taken as the instantaneous rain rate as follows:

$$\mathrm{rr} = \max(\mathrm{bf}R_{19V}, \mathrm{bfbr}R_{37V}). \quad (3)$$

The use of maximum of two channel's rain rates is based on the assumption that problems in the retrieval such as beamfilling, saturation, or scattering by ice particles will generally cause an underestimate of the rain rate. The larger of the two rain rates is presumably less affected by these problems and thereby a better estimate. The factor bf is the beamfilling error correction factor. Beamfilling error results from nonuniform rain rates within a field of view (FOV) and the nonlinear *T–R* relationship. It causes retrieved rain rates to be lower than true rain rates. Previous studies (Chiu et al. 1990; Short and North 1990) suggested that the beamfilling error could be corrected by multiplying the retrieved rain rate by a single factor. This study uses the factor of 1.8 for the 19.35-GHz channel, which was derived from simulation studies using the Global Atmospheric Research Program (GARP) Atlantic Tropical Experi-

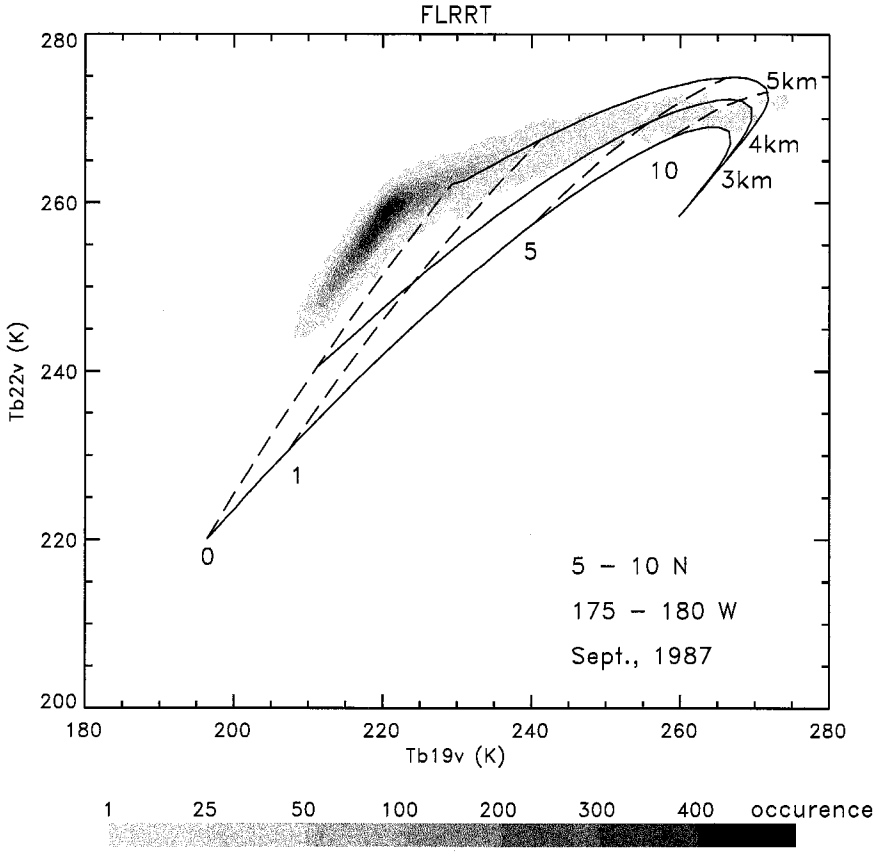

FIG. 2. Two-dimensional histogram of brightness temperatures from 19V and 22V channels over a 5° × 5° box in the ITCZ. Isolines of freezing level (solid lines) and rain rate (dashed lines) calculated from *T–R* relationships are overlaid.

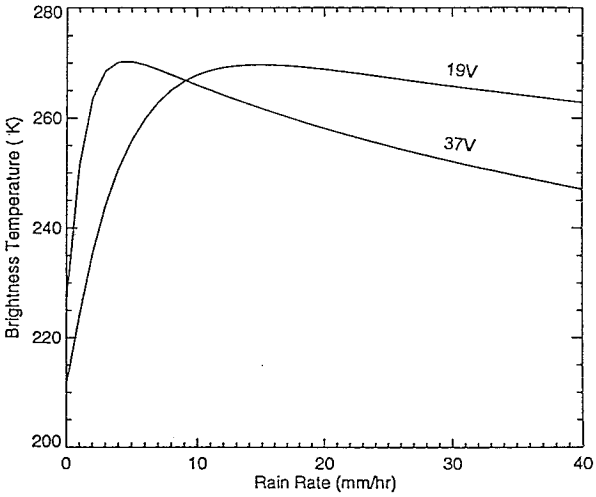

FIG. 3. The *T–R* relationships for the 19V and 37V channels with a 4-km freezing level.

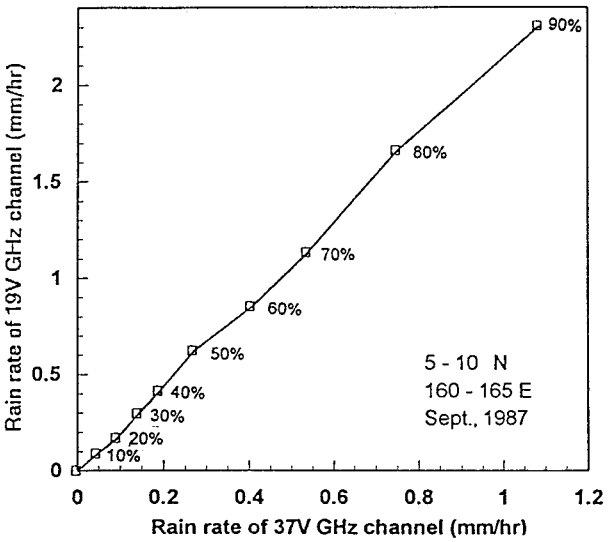

FIG. 4. Cumulative rain-rate probabilities of the 19V and 37V channels for 5°–10°N, 160°–165°E, September 1987.

ment (GATE) data (Wilheit et al. 1991). We have no intention here to improve individual pixel estimates with this beamfilling correction. The beamfilling correction can only correct for the average bias over an ensemble of rainfall estimates such as might be used for time–area averages.

The factor br, which is only applied to R_{37V}, is the beamfilling factor of R_{37V} *relative* to that of R_{19V}. Since the *T–R* relationship for the 37-GHz channel has a larger nonlinearity than that for 19-GHz channel, the beamfilling error of R_{37V} will be larger than that of R_{19V} even though the 37-GHz channel has a higher spatial resolution. Thus, the retrieved R_{37V} will be lower than R_{19V}. In order to estimate the ensemble difference between R_{19V} and R_{37V}, a statistical comparison of R_{19V} and R_{37V} was performed. Figure 4 shows the cumulative rain-rate probabilities for the 19V and 37V channels. The square points correspond to every 10th percentile of rain intensity. We can see that R_{19V} is approximately twice the value of R_{37V} up to the 90th percentile rain pixel. Since the actual rainfall is the same for both sets of retrievals, there is a factor of 2 for R_{37V} values relative to R_{19V}. The factor of 2 is a typical value for rain areas in the Tropics and thus is applied to R_{37V}. It may not be true in the subtropics and part of the midlatitudes where rainfall usually is not as heavy as that in the Tropics. Exactly how to combine the observations at multiple frequencies and resolutions is still an open issue; this can only be considered an initial attempt.

In application, the freezing level is determined by a simultaneous solution of the *T–R* relationships at 19.35 and 22.235 GHz (vertical polarization) for a given pair of observations. This solution is implemented via a look-up table for computational efficiency. With the freezing level so determined, it is then straightforward to solve for a rain rate using the 19.35- and 37-GHz observations. Because the *T–R* relationships decrease at very high rain rates, this solution is double valued; the lower rain-rate value is taken as the solution.

b. Estimate of monthly rainfall

Estimation of monthly rainfall totals over the oceans is important for climatological studies. Simply averaging the instantaneous rain rates for one month may not accurately represent the true distribution of a monthly rainfall because of the limited dynamic range of the underlying measurement technique. Moreover, even with a perfect measurement technique, the very high rain rates, being infrequent, would be poorly sampled with observations from a low orbiting satellite. However, if we have an estimate of the *form* of the probability distribution of rain rates, we can estimate the contribution to the rain rates outside of our dynamic range by extrapolation.

Examining data from GATE, Kedem and Chiu (1987) found that rainfall closely fits a mixed lognormal distribution both spatially and temporally. Kedem et al. (1990) also showed that a mixed lognormal distribution fits the rainfall data better than a gamma distribution. The assumption of a mixed lognormal distribution of rainfall intensity is adopted for the current study.

1) A MIXED LOGNORMAL DISTRIBUTION

Since most pixels in a $5° \times 5°$ box contain no rain and a lognormal distribution holds only for nonzero rainfall, a mixed lognormal distribution (the combination of a delta function at zero and a lognormal distribution for nonzero rainfall) has to be considered. Kedem et al. (1990) have discussed the mixed distribution of rainfall. It can be expressed as

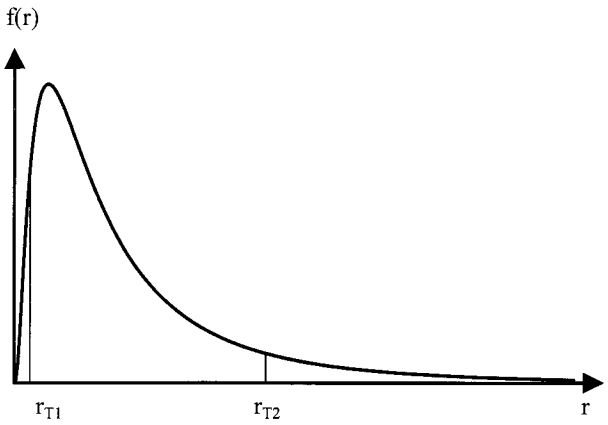

FIG. 5. A lognormal distribution. Here, r_{T1} and r_{T2} are fixed truncation points.

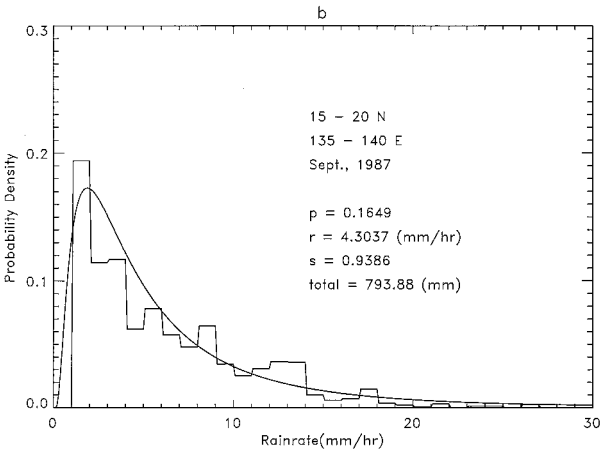

FIG. 6. Histogram and fitted lognormal curves for 15°–20°N, 135°–140°E, September 1987.

$$g(r) = \begin{cases} (1 - p)\delta(r) & r \le 0, \\ pf(r) & r > 0, \end{cases} \tag{4}$$

where p is the probability of a rain event and

$$f(r) = \frac{1}{\sqrt{2\pi}\sigma r} \exp\left\{-\frac{[\ln(r/r_0)]^2}{2\sigma^2}\right\}, \tag{5}$$

where $f(r)$ is the probability of a given rain rate, r; r_0 is the logarithmic mean rain rate; and σ is the standard deviation of the logarithm of rain rate.

The mean rain rate and variance of a mixed lognormal distribution are as follows:

$$E(R) = pr_0 \exp(\sigma^2/2) \tag{6}$$

$$\text{var}(R) = pr_0 \exp(\sigma^2)[\exp(\sigma^2) - p], \tag{7}$$

where R indicates a rain event.

2) ESTIMATION OF PARAMETERS p, r_0, AND σ

The coefficients p, r_0, and σ are determined by fitting the observed rain-rate distribution to the lognormal form using a maximum likelihood estimation method. This method has been described in detail by Aitchison and Brown (1957) and Cohen (1991). For untruncated rain-rate samples consisting of observations r_i, $i = 1, \ldots, n_t$, the likelihood function of a mixed lognormal distribution is

$$L = \prod_{i=1}^{n_t} g(r_i; p, r_0, \sigma) = (1 - p)^{n_0} p^{n_r} \prod_{i=1}^{n_r} f(r_i), \tag{8}$$

where n_0: number of nonraining pixels; n_r: number of raining pixels; and n_t: total number of pixels, $n_t = n_0 + n_r$. To obtain maximum likelihood estimates of p, r_0, and σ, we take the logarithms of Eq. (8), differentiate with respect to these parameters, and equate to zero. The results are as follows:

$$p = \frac{n_r}{n_t}. \tag{9}$$

$$\ln(r_0) = \frac{1}{n_r} \sum_{i=1}^{n_r} \ln(r_i). \tag{10}$$

$$\sigma^2 = \frac{1}{n_r} \sum_{i=1}^{n_r} [\ln(r_i) - \ln(r_0)]^2. \tag{11}$$

As mentioned before, a severe limitation of emission-based methods is that rain rates are reliably retrieved only over a limited dynamic range. The fit is likewise limited to the reliable portion of the dynamic range. Sample data that can only be observed or measured in certain regions

TABLE 2. Examples of estimated parameters p, r_0, and σ.

Time	Latitude	Longitude	p	r_0 (mm h^{-1})	σ (mm h^{-1})	Total (mm)
Aug 1987	5°–10°N	120°–125°W	0.2203	1.4563	1.1187	431.87
Aug 1987	5°–10°N	145°–150°E	0.1336	2.5237	0.9226	371.61
Sep 1987	10°–15°N	150°–155°E	0.0882	2.8428	1.0452	311.69
Sep 1987	10°–15°N	165°–170°E	0.1233	1.1591	1.2952	238.14
Oct 1987	0°–5°N	155°–160°W	0.0650	1.1664	1.0940	99.37
Oct 1987	0°–5°N	85°–90°E	0.1550	1.5950	1.0764	317.61
Nov 1987	0°–5°S	70°–75°E	0.0415	2.5568	0.9609	121.23
Nov 1987	5°–10°S	150°–155°W	0.0312	2.7864	1.2394	135.07
Aug 1989	10°–15°N	115°–120°E	0.1071	2.4909	0.9319	296.42
Sep 1989	5°–10°N	85°–90°E	0.2857	1.1763	1.1638	476.39

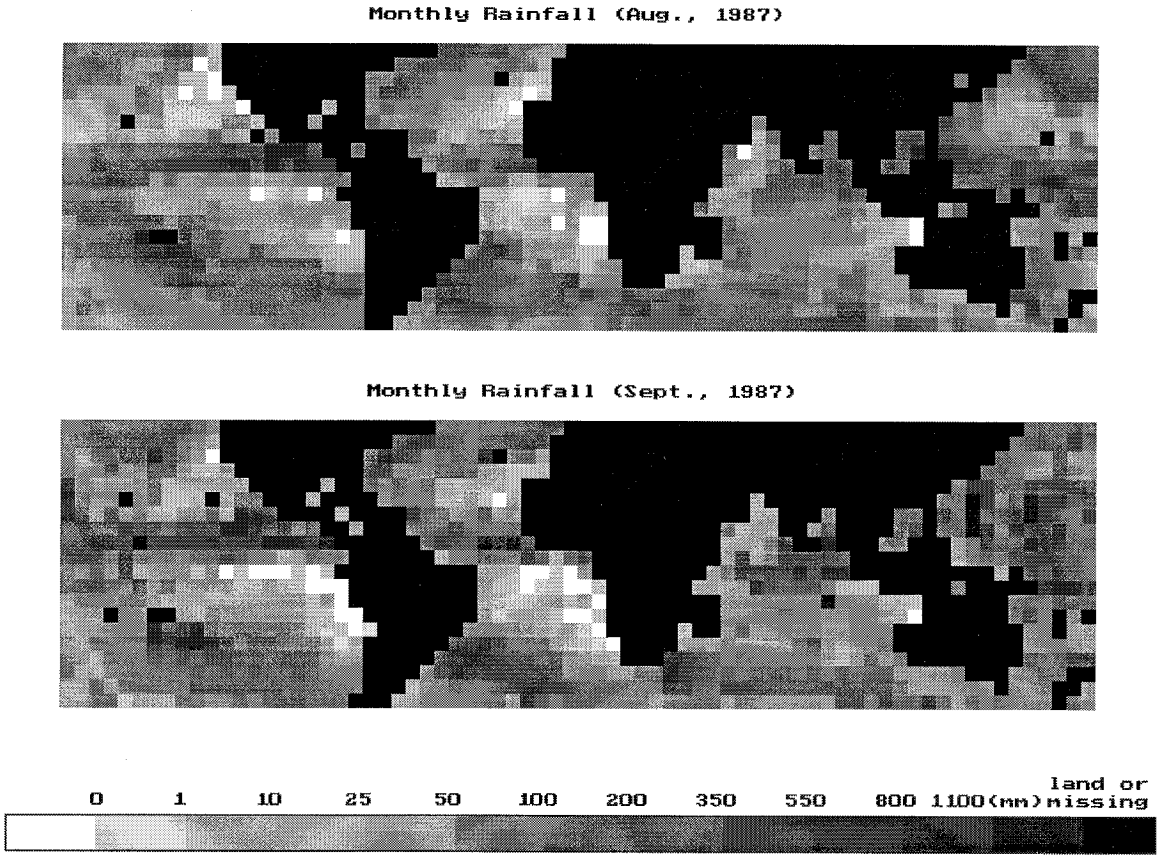

FIG. 7. Monthly rainfall on 5° × 5° boxes for August, September, October, and November 1987.

of sample space are called truncated sample data. Figure 5 shows a lognormal distribution of rainfall with the fixed truncation points at r_{T1} and r_{T2}. Truncated samples have three cases: (a) left truncation, in which sample data with values less than r_{T1} are truncated; (b) right truncation, in which sample data with values larger than r_{T2} are truncated; and (c) double truncation, which includes cases (a) and (b).

Therefore, we can say the samples of instantaneous rain rates are doubly truncated at r_{T1} and r_{T2} for heavy rainfall. With the frequency range from 19 to 37 GHz, the r_{T2} is approximately 20.0 mm h^{-1} (after applying the beamfilling correction). Previous studies (Wilheit 1994) have suggested that r_{T1} is about 1.0 mm h^{-1}. For light rainfall, the rain-rate samples are complete at the right side and hence are only left truncated at 1.0 mm h^{-1}. The maximum likelihood estimation method must be modified in the cases of truncated rain-rate samples.

For left truncated samples, the analytical solutions of r_0 and σ can be derived from maximum likelihood estimation equations. They are given by

$$\ln(r_0) = \bar{r} - \theta(\alpha)[\bar{r} - \ln(r_{T1})], \tag{12}$$

and

$$\sigma^2 = s^2 + \theta(\alpha)[\bar{r} - \ln(r_{T1})]^2, \tag{13}$$

where

$$\bar{r} = \frac{1}{n}\sum_{i=1}^{n} \ln(r_i), \tag{14}$$

$$s^2 = \frac{1}{n}\sum_{i=1}^{n} [\ln(r_i) - \bar{r}]^2, \tag{15}$$

$$\theta(\alpha) = \theta(\xi) = \frac{Q(\xi)}{Q(\xi) - \xi}, \tag{16}$$

$$\alpha = \frac{s^2}{[\bar{r} - \ln(r_{T1})]^2}, \tag{17}$$

$$\xi = \frac{\ln(r_{T1}/r_0)}{\sigma}, \tag{18}$$

and

$$Q(\xi) = \frac{\varphi(\xi)}{1 - \Phi(\xi)}, \tag{19}$$

where n is the number of truncated rain-rate samples, $\theta(\alpha)$ is the auxiliary estimation function, and $\phi(\xi)$ and $\Phi(\xi)$ are probability distribution function and cumulative distribution function of the standard normal distribution, respectively.

The table for the auxiliary estimation function $\theta(\alpha)$ has been given by Cohen (1959). In application, it is necessary

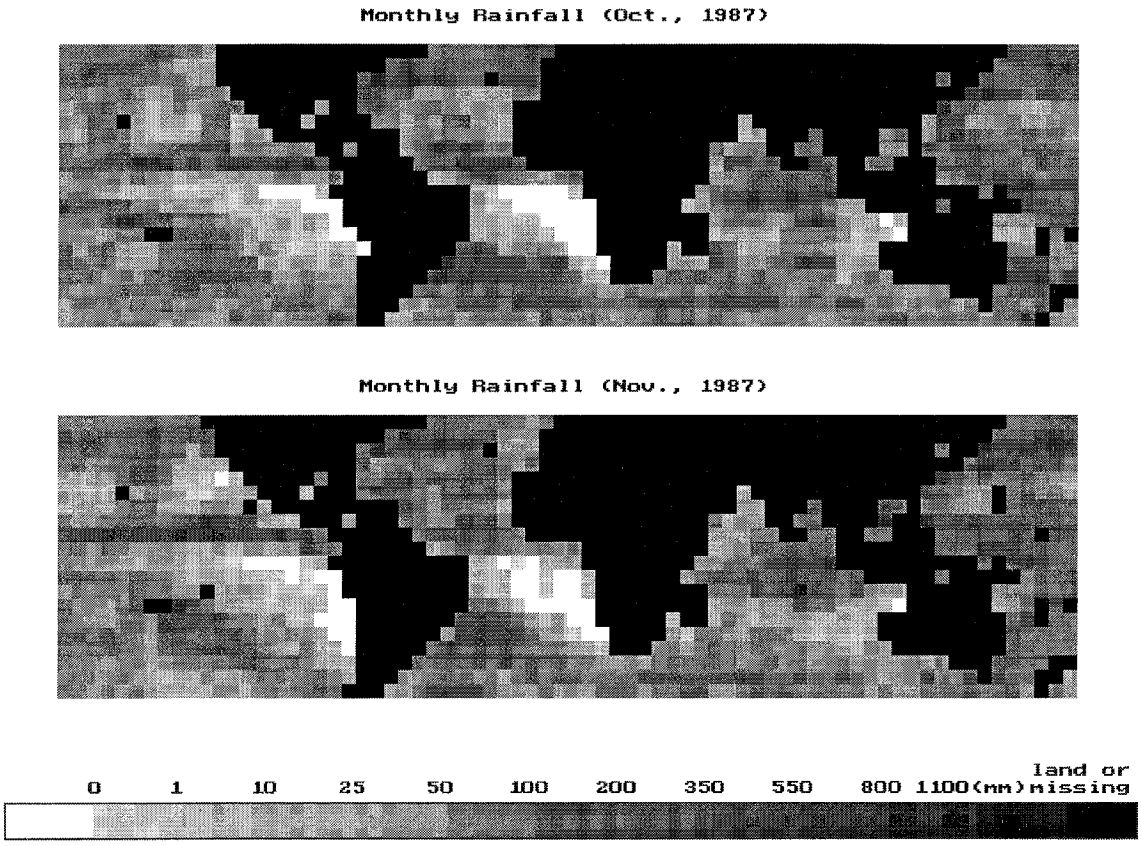

FIG. 7. (*Continued*)

only that we calculate $\bar{r}$ and s^2 from rain-rate samples. Then σ^2 and $\ln(r_0)$ are calculated from Eqs. (12) and (13). With r_0 and σ, the parameter p can be estimated by

$$p = \frac{n}{n_r \int_{r_{T1}}^{\infty} f(r)\, dr}. \tag{20}$$

Unlike the singly left truncated rain-rate samples, an analytical solution is difficult for doubly truncated rain-rate samples. Therefore, only numerical solutions can be obtained. Here, σ, r_0, and p can be expressed as follows:

$$\sigma = \frac{\ln(r_{T2}) - \ln(r_{T1})}{\xi_2 - \xi_1}, \tag{21}$$

$$r_0 = \exp[\ln(r_{T1}) - \sigma\xi_1], \tag{22}$$

and

$$p = \frac{n}{n_r \int_{r_{T1}}^{r_{T2}} f(r)\, dr}, \tag{23}$$

where

$$\xi_1 = \frac{\ln(r_{T1}/r_0)}{\sigma} \tag{24}$$

and

$$\xi_2 = \frac{\ln(r_{T2}/r_0)}{\sigma}. \tag{25}$$

Here, ξ_1 and ξ_2 can be solved numerically from maximum likelihood estimation equations.

4. Application to SSM/I data

Histograms of instantaneous rain rates at 1.0 mm h^{-1} increments from 0.0 to 40.0 m h^{-1} have been collected in $5^\circ \times 5^\circ$ boxes over oceans for each month from August through November 1987 and from January through December 1989. For each $5^\circ \times 5^\circ$ box, there are about 16 000 pixels. If more than 25% of the pixels in one box are located over land, this box will be considered a land area and rainfall will not be calculated. If there are too few raining pixels in one box ($\leq$100) to be used with any confidence, the monthly rainfall is calculated by simply averaging the observations. For normal situations, the r_0, σ, and p can be estimated using the equations described

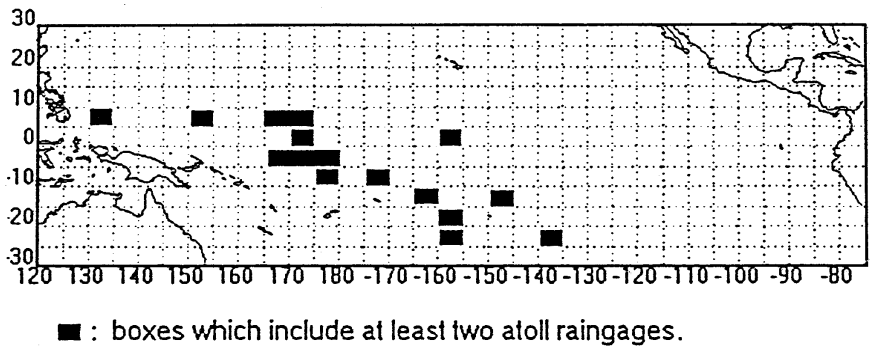

FIG. 8. The 5° × 5° boxes that include at least two atoll stations.

in section 3. Table 2 gives some partial results. Figure 6 shows one sample of the histogram and fitted curve.

Monthly rainfall totals are computed by multiplying the averaged rain rates estimated from Eq. (3) by the number of hours in one month. The global patterns of monthly rainfall for August, September, October, and November 1987 are displayed in Fig. 7. The figures clearly show the tropical large-scale features such as heavy rainfall along ITCZ and SPCZ.

Comparison of monthly rainfall between satellite estimates and the atoll data has been performed. Although the density of atoll rain gauge data is not sufficient for accurately validating the satellite observations, they are the best ground truth data available so far. Atoll data were first averaged into 5° × 5° boxes. In order to reduce the spatial sampling error between the satellite estimates and the atoll data, only those boxes that included at least two rain gauge data were utilized. Figure 8 displays the 5° × 5° boxes that have at least two rain gauges.

Since minimal atoll data are available for 1989, the comparisons are based on seasons [January, February, March (JFM); April, May, June (AMJ); July, August, September (JAS); and October, November, December (OND)], while monthly comparison statistics were calculated for 1987. There are approximately 10 5° × 5° boxes of atoll data for each case. Table 3 gives means of atoll rainfall and estimated satellite rainfall, mean error, root-mean-square (rms) error, and correlation coefficient between the atoll rainfall data and the satellite-estimated rainfall data. Two scatterplots of the SSM/I inferred rainfall versus the atoll rainfall data are displayed in Fig. 9. Except in JFM 1989, all cases have high correlation and reasonable mean and rms errors. These validation results indicate that this algorithm performs quite well in tropical areas, especially in September 1987 and JAS 1989.

TABLE 3. Statistical results of validation.

Month	No. of data	Mean of atoll data (mm)	Mean of est. rainfall (mm)	Mean error (mm)	rms error (mm)	Corr. coeff.
Aug 1987	12	242.71	213.70	−29.01	101.40	0.681
Sep 1987	11	174.88	154.26	−20.62	51.02	0.914
Oct 1987	10	252.64	169.15	−83.49	99.78	0.862
Nov 1987	9	184.28	134.62	−49.66	74.06	0.835
Jan–Mar 1989	14	162.81	125.05	−37.76	91.65	0.215
Apr–Jun 1989	14	256.56	236.23	−20.33	88.47	0.720
Jul–Sep 1989	13	216.75	238.72	21.97	86.00	0.862
Oct–Dec 1989	15	233.01	218.97	−14.04	74.50	0.688
Total	98	221.43	188.59	−32.84	97.79	0.689

5. Summary and conclusions

A physical–statistical approach has been developed that uses an emission-based method to retrieve instantaneous rain rates and computes monthly rainfall employing a maximum likelihood estimate method on a limited rain-rate dynamic range. The beamfilling error is corrected by multiplying a factor of 1.8, which is generated from simulation studies of GATE data.

Global patterns of monthly rainfall clearly display tropical large-scale features such as the ITCZ and SPCZ. Comparison with Pacific atoll data indicates this algorithm performs very well in tropical areas. The good agreement with the atoll data, however, is imperfect. There are many potential reasons for the discrepancy. The atolls may well not be representative of the oceanic areas within the 5° × 5° boxes. A diurnal cycle of rainfall, if it contains harmonics of a single daily cycle, can introduce a bias if the rain is only sampled at two times of the day separated by 12 h, as is the case for tropical observations from a sun-synchronous satellite. The magnitude and even the sign of the bias will depend on the details of the higher-order harmonics in the diurnal cycle and the timing of the sun-synchronous observations. The future TRMM satellite will have a non-sun-synchronous orbit specifically to permit sampling of the diurnal cycle.

It would be tempting to adjust some parameter of the retrieval (for instance, the beamfilling correction) to make the retrievals agree with the atoll data or some other so-called ground truth data. We do not believe this would be wise or reasonable. Oceanic rain is extraordinarily difficult to measure by any means. There is no reason to believe that the ground truth represents the actual rainfall any better than do the retrievals. It seems more reasonable to

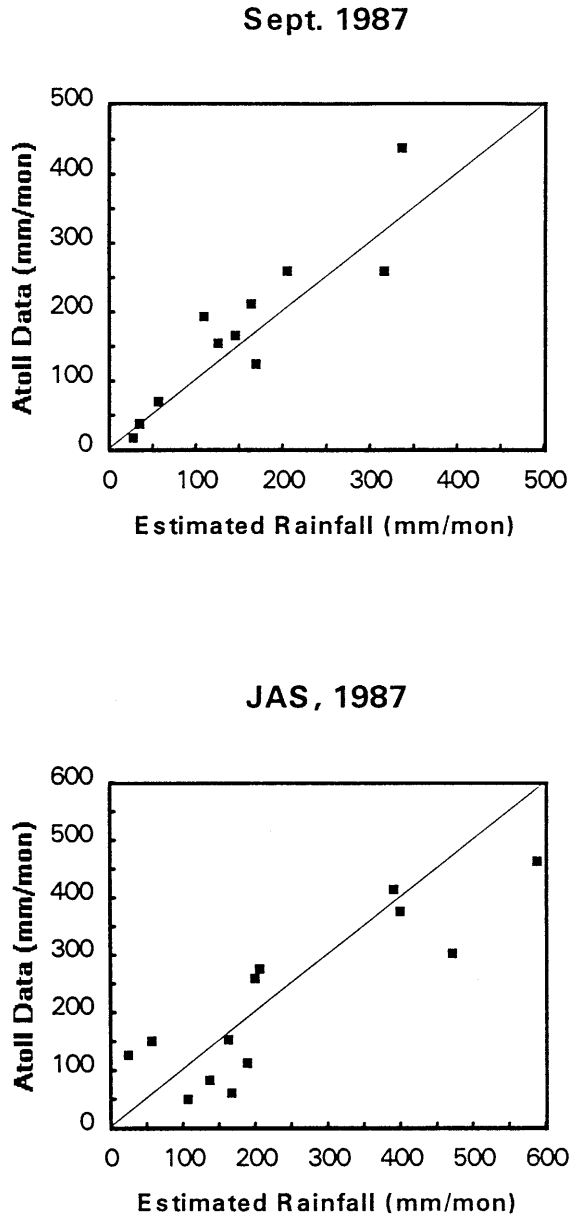

FIG. 9. The scatterplots of the SSM/I inferred rainfall vs the atoll rainfall data for (a) September 1987 and (b) JAS 1989.

make the physics and logic of the retrieval as realistic as we can and only depend on comparisons with ground truth to detect egregious errors.

Does this algorithm represent an improvement over other rainfall-retrieval algorithms? It would be convenient if there were some benchmark for algorithm performance. Experience at the various rainfall algorithm intercomparisons has made it abundantly clear that there is no such benchmark for oceanic rainfall. At this point, the best that can be achieved is to compare with datasets, such as the Pacific atoll set used here, to check for reasonableness and then attempt to judge the self-consistency of the physics used in the retrieval, which is a very subjective process. Here, we are attempting to address the limited dynamic range of the measurements by using the assumption that the rainfall intensity is lognormally distributed to estimate the contributions from above and below the dynamic range of the measurements by extrapolation. In examining the full set of our retrievals reported here, we find that for about 10% of the cells the contribution of rain rates greater than 20 mm h^{-1} exceeded 35% of the total and in another 10% the contribution from rain rates lower than 1 mm h^{-1} represented 10% of the rainfall total. Clearly, the contribution from high rain rates is important and must be more accurately approximated than the face value of the measurements will permit. On the other hand, the importance of the rain rates below the minimum measurable rate is marginal, at least for the latitude range studied here.

As an experiment, the cells that were used for the comparison with the atoll dataset were reanalyzed, but the dynamic range issues were ignored. The retrieved rain rates (after beamfilling corrections) were taken at face value in the computation of the lognormal parameters, that is, an analog of the Berg and Chase (1992) method. The rainfall totals were reduced in all cases by factors ranging from 0.80 to 0.83. Because of saturation effects, the contribution of high rain rates is systematically underestimated; the method discussed here addresses this underestimate.

With the launch of TRMM (planned for 1997), we will have observations at the same frequencies but with much better spatial resolution (roughly a factor of 6 in area). The beamfilling corrections will be smaller with less uncertainty. The improved resolution will also modify the observed rainfall distributions. The probability of rainfall p will decrease, and the log-mean rain rate r_0 will increase. The log-variance σ^2 may also change. As a result, the contribution of rain rates below the 1 mm h^{-1} minimum will become even less significant, while the contribution from high rain rates will become even more significant. TRMM will also have a 10.7-GHz channel that will increase the upper limit on the dynamic range by roughly a factor of 4, but at a degraded spatial resolution.

More work is needed in order to improve this algorithm, such as modification of simple plane-parallel cloud models, further studies on beamfilling error, the addition of data from infrared radiometers, and other operational SSM/I to improve the poor spatial and temporal samplings. The selection of truncated rain-rate points will also affect the monthly rainfall because this algorithm works well only if a small percentage of the samples have been truncated. It should also be possible to generalize the maximum likelihood estimator to operate on several histograms simultaneously so that the information from all the channels could be used wherever their dynamic ranges overlapped.

Acknowledgments. The authors would like to thank Drs. Al Chang, Long Chiu, and Jeff Tesmer for many useful discussions and Mr. Hugh Powell for providing the SSM/I data and helping the first author remotely access those

data. Constructive comments provided by three anonymous reviewers are deeply appreciated. This study was partially supported by NASA Grant NAG5-1568.

REFERENCES

Aitchison, J., and J. A. C. Brown, 1957: *The Lognormal Distribution.* Cambridge University Press, 176 pp.

Berg, W., and R. Chase, 1992: Determination of mean rainfall from the Special Sensor Microwave/Imager (SSM/I) using a mixed lognormal distribution. *J. Atmos. Oceanic Technol.,* **9,** 129–141.

Chiu, L. S., G. R. North, D. A. Short, and A. McConnell, 1990: Rain estimation from satellites: Effect of finite field of view. *J. Geophys. Res.,* **95,** 2177–2185.

Cohen, A. C., 1959: Simplified estimators for the normal distribution when samples are singly censored or truncated. *Technometrics,* **1,** 217–237.

——, 1991: *Truncated and Censored Samples: Theory and Applications.* Marcel Dekker, 312 pp.

Hollinger, J., R. Lo, and G. Poe, 1987: Special Sensor Microwave/Imager user's guide. Space Sensing Branch, Naval Research Laboratory, Washington, DC, 177 pp.

Huang, R., and K.-N. Liou, 1983: Polarized microwave radiation transfer in precipitating cloudy atmospheres: Applications to window frequencies. *J. Geophys. Res.,* **88,** 3885–3893.

Kedem, B., and L. S. Chiu, 1987: On the lognormality of rain rate. *Proc. Natl. Acad. Sci. U.S.A.,* **84,** 901–905.

——, ——, and G. R. North, 1990: Estimation of mean rain rate: Application to satellite observations. *J. Geophys. Res.,* **95,** 1965–1972.

Kummerow, C., and J. A. Weinman, 1988: Determining microwave brightness temperatures from precipitating horizontally finite and vertically structured clouds. *J. Geophys. Res.,* **93,** 3720–3728.

——, and L. Giglio, 1994a: A passive microwave technique for estimating rainfall and vertical structure information from space. Part I: Algorithm description. *J. Appl. Meteor.,* **33,** 3–18.

——, and ——, 1994b: A passive microwave technique for estimating rainfall and vertical structure information from space. Part II: Applications to SSM/I data. *J. Appl. Meteor.,* **33,** 19–33.

——, R. A. Mack, and I. M. Hakkarinen, 1989: A self-consistency approach to improve microwave rainfall rate estimation from space. *J. Appl. Meteor.,* **28,** 869–884.

——, I. M. Hakkarinen, H. F. Pierce, and J. A. Weinman, 1991: Determination of precipitation profiles from airborne passive microwave radiometric measurements. *J. Atmos. Oceanic Technol.,* **8,** 148–158.

McGaughey, G., E. J. Zipser, R. W. Spencer, and R. E. Hood, 1996: High resolution passive microwave observations of convective systems over the tropical Pacific Ocean. *J. Appl. Meteor.,* **35,** 1921–1947.

Morrissey, M. L., and J. S. Green, 1991: The Pacific Atoll Raingage Data Set. Tech. Rep., University of Hawaii at Manoa, Honolulu, HI. [Available from University of Hawaii at Manoa, Honolulu, HI 96822.]

Mugnai, A., and E. A. Smith, 1988: Radiative transfer to space through a precipitating cloud at multiple microwave frequencies. Part I: Model description. *J. Appl. Meteor.,* **27,** 1055–1073.

——, ——, and G. J. Tripoli, 1993: Foundations for statistical–physical precipitation retrieval from passive microwave satellite measurements. Part II: Emission-source and generalized weighting-function properties of a time-dependent cloud-radiation model. *J. Appl. Meteor.,* **32,** 17–39.

Olson, W. S., 1987: Estimation of rainfall rates in tropical cyclones by passive microwave radiometry. Ph.D. dissertation, University of Wisconsin–Madison, 292 pp.

——, 1989: Physical retrieval of rainfall rates over the ocean by multispectral microwave radiometry: Application to tropical cyclones. *J. Geophys. Res.,* **94,** 2269–2280.

Petty, G. W., and K. B. Katsaros, 1990: Precipitation observed over the South China Sea by the Nimbus-7 scanning multichannel microwave radiometer during winter MONEX. *J. Appl. Meteor.,* **29,** 273–287.

Prabhakara, C., D. A. Short, W. Wiscombe, R. S. Fraser, and B. E. Vollmer, 1986: Rainfall over oceans inferred from Nimbus-7 SMMR: Application to 1982–83 El Niño. *J. Climate Appl. Meteor.,* **25,** 1464–1475.

Rodgers, E. B., and H. Siddalingaiah, 1983: The utilization of Nimbus-7 SMMR measurements to delineate rainfall over land. *J. Climate Appl. Meteor.,* **22,** 1753–1763.

Shin, K. S., P. E. Riba, and G. R. North, 1990: Estimation of area-averaged rainfall over tropical oceans from microwave radiometry: A single channel approach. *J. Appl. Meteor.,* **29,** 1031–1042.

Short, D. A., and G. R. North, 1990: The beam filling error in the Nimbus-5 electronically scanning microwave radiometer observations of Global Atlantic Tropical Experiment rainfall. *J. Geophys. Res.,* **95,** 2187–2193.

Simpson, J. R., R. Adler, and G. R. North, 1988: A proposed tropical rainfall measuring mission (TRMM). *Bull. Amer. Meteor. Soc.,* **69,** 278–295.

Smith, E. A., and A. Mugnai, 1988: Radiative transfer to space through a precipitating cloud at multiple microwave frequencies. Part II: Results and analysis. *J. Appl. Meteor.,* **27,** 1074–1091.

——, ——, H. J. Cooper, G. J. Tripoli, and X. Xiang, 1992: Foundations for statistical–physical precipitation retrieval from passive microwave satellite measurements. Part I: Brightness-temperature properties of a time-dependent cloud-radiation model. *J. Appl. Meteor.,* **31,** 506–531.

Spencer, R. W., 1986: A satellite passive 37-GHz scattering-based method for measuring oceanic rain rates. *J. Climate Appl. Meteor.,* **25,** 754–766.

——, D. W. Martin, B. B. Hinton, and J. A. Weinman, 1983: Satellite microwave radiances correlated with radar rain rates over land. *Nature,* **304,** 141–143.

——, H. M. Goodman, and R. E. Hood, 1989: Precipitation retrieval over land and ocean with the SSM/I: Identification and characteristics of the scattering signal. *J. Atmos. Oceanic Technol.,* **6,** 254–273.

Tesmer, J. R., 1995: An improved microwave radiative transfer model for tropical oceans. Ph.D. dissertation, Texas A&M University, 87 pp.

Wang, S. A., 1996: Modeling the beamfilling correction for microwave retrieval of oceanic rainfall. Ph.D. dissertation, Texas A&M University, 100 pp.

Weinman, J. A., and P. J. Guetter, 1977: Determination of rainfall distributions from microwave radiation measured by the Nimbus-6 ESMR. *J. Appl. Meteor.,* **16,** 437–442.

Wilheit, T. T., 1986: Some comments on passive microwave measurement of rain. *Bull. Amer. Meteor. Soc.,* **67,** 1226–1232.

——, 1994: Algorithms for the retrieval of rainfall from passive microwave measurements. *Remote Sens. Rev.,* **11,** 163–194.

——, A. T. C. Chang, M. S. V. Rao, E. B. Rodgers, and J. S. Theon, 1977: A satellite technique for quantitatively mapping rainfall rates over the oceans. *J. Appl. Meteor.,* **16,** 551–560.

——, ——, J. L. King, E. B. Rodgers, R. A. Nieman, B. M. Krupp, A. S. Milman, J. S. Stratigos, and H. Siddalingaiah, 1982: Microwave radiometric observations near 19.35, 92, and 183 GHz of precipitation in tropical storm Cora. *J. Appl. Meteor.,* **21,** 1137–1145.

——, ——, and L. S. Chiu, 1991: Retrieval of monthly rainfall indices from microwave radiometric measurements using probability distribution functions. *J. Atmos. Oceanic Technol.,* **8,** 118–136.

Wu, R., and J. A. Weinman, 1984: Microwave radiances from precipitating clouds containing aspherical ice, combined phase, and liquid hydrometeors. *J. Geophys. Res.,* **89,** 7170–7178.